UNIVERSITY OF LEEDS

This is a repository copy of *Solidification of Undercooled Melts of Al-Based Alloys on Earth and in Space*.

White Rose Research Online URL for this paper:
http://eprints.whiterose.ac.uk/117572/

Version: Accepted Version

Article:
Herlach, DM, Burggraf, S, Galenko, P et al. (7 more authors) (2017) Solidification of Undercooled Melts of Al-Based Alloys on Earth and in Space. JOM, 69 (8). pp. 1303-1310. ISSN 1047-4838

https://doi.org/10.1007/s11837-017-2402-y

(c) 2017, The Minerals, Metals & Materials Society. This is an author produced version of a paper published in JOM. Uploaded in accordance with the publisher's self-archiving policy. The final publication is available at Springer via https://doi.org/10.1007/s11837-017-2402-y

Reuse
Items deposited in White Rose Research Online are protected by copyright, with all rights reserved unless indicated otherwise. They may be downloaded and/or printed for private study, or other acts as permitted by national copyright laws. The publisher or other rights holders may allow further reproduction and re-use of the full text version. This is indicated by the licence information on the White Rose Research Online record for the item.

Takedown
If you consider content in White Rose Research Online to be in breach of UK law, please notify us by emailing eprints@whiterose.ac.uk including the URL of the record and the reason for the withdrawal request.

White Rose university consortium
Universities of Leeds, Sheffield & York

eprints@whiterose.ac.uk
https://eprints.whiterose.ac.uk/

Solidification of Undercooled Melts of Al-based Alloys on Earth and in Space

Dieter M. Herlach[1)2)], Stefan Burggraf[1)2)], Peter Galenko[3)], Charles-André Gandin[4)], Asuncion Garcia-Escorial[5)], Hani Henein[6)], Christian Karrasch[)2)], Andrew Mullis[7)], Markus Rettenmayr[3),] Jonas Valloton [6)]

1) Institut für Materialphysik im Weltraum, Deutsches Zentrum für Luft- und Raumfahrt, D-51170 Köln, Germany
2) Institut für Experimentalphysik IV, Ruhr-Universität Bochum, D-44780 Bochum, Germany
3) Otto-Schott-Institut für Materialforschung, Friedrich-Schiller-Universität Jena, Löbdergraben 32, D-07743 Jena, Germany
4) MINES ParisTech, CEMEF-UMR CNRS 7635, 1 rue Claude Daunesse – CS 10207, F-06904 Sophia Antipolis Cedex, France
5) Metalurgia Fisica, CENIM-CSIC, Avda. Gregorio del Amo 8, E-28040 Madrid, Spain
6) Department of Chemical and Materials Engineering, University of Alberta, Edmonton T6G 1H9, Canada
7) School of Chemical and Process Engineering, University of Leeds, Leeds LS2-9JT, United Kingdom

Abstract

Containerless processing of droplets and drops by atomization and electromagnetic levitation are applied to undercool metallic melts and alloys prior to solidification. Heterogeneous nucleation on crucible walls is completely avoided giving access to large undercoolings. Experiments are performed both under terrestrial (1g) conditions and in reduced gravity (µg) as well. Microgravity conditions are realized by the free fall of small droplets during atomization of a spray of droplets, individual drops in a drop tube and by electromagnetic levitation of drops during parabolic flights, sounding rocket missions and using the Electro-Magnetic Levitator EML multi-user facility on board the International Space Station ISS. The comparison of both sets of experiments in 1g and µg leads to an estimation of the influence of forced convection on dendrite growth kinetics and microstructure evolution

Corresponding author: dieter.herlach@dlr.de

1. Introduction

Metallic materials are prepared from the liquid state as their parent phase. To date, efforts are directed towards virtual material design with computer assisted modelling. Computational materials science from the liquid state requires detailed knowledge of crystal nucleation and crystal growth. Both processes are driven by an undercooling of the liquid below its equilibrium melting temperature. At large undercoolings this gives access to non-equilibrium solidification pathways, which can form metastable solids, which may differ in their physical and chemical properties from their stable counterparts.

To achieve the state of a deeply undercooled melt heterogeneous nucleation has to been reduced. Turnbull used the method of volume separation of heterogeneous sites by sample subdivision into many small particles in order to isolate the heterogeneous motes in a few particles [1]. Perepezko refined this technique by subdividing the macroscopic melt into small particles suspended in an inert carrier fluid. The carrier fluid acts as an agent removing heterogeneous motes on the surface of the small droplets as well [2]. Even undercooling of macroscopic melts in a fluxing agent can be used to achieve very large undercoolings enabling the formation of bulk glass formation of metallic alloy [3, [4]. During the last decades, levitation techniques are progressively used to produce liquid drops of metals, alloys and semiconducturs. These techniques offer the additional benefit that a freely suspended drop is directly accessible for in situ diagnostics to determine thermophysical properties and investigate solidification far away from thermodynamic equilibrium.

In the present paper an overview is given by the partners of the NEQUISOL[1] project funded by the European Space Agency. Solidification is studied under the conditions of containerless processing on Earth and in reduced gravity [5]. A sophisticated impulse atomization facility is used to produce a spray of droplets. Atomization is very suitable to investigate the statistics of the formation of various structures and microstructures as a function of droplet size and cooling rate. However, these techniques do not allow for direct diagnostics of individual droplets. For this purpose, we apply electromagnetic levitation on Earth and in reduced gravity [6]. Comparing results obtained under terrestrial and reduced gravity conditions allows the investigation of fluid flow effects in dendrite growth dynamics and in the microstructure evolution of solidification. The experiments are accompanied by the dvelopment and application of mesoscopic models to analyse solidification including fluid flow by forced convection [7].

2. Experiments

In the present project, methods of containerless processing are applied to undercool metallic melts without any contact with a solid crucible. That allows for deep undercoolings and solidification far away from equilibrium. These techniques include gas atomization, impuls atomization drop tube, melt fluxing, and electromagnetic levitation both on Earth and in Space. Most of the experimental techniques used within the NEQUISOL project are described in detail elsewhere [8].

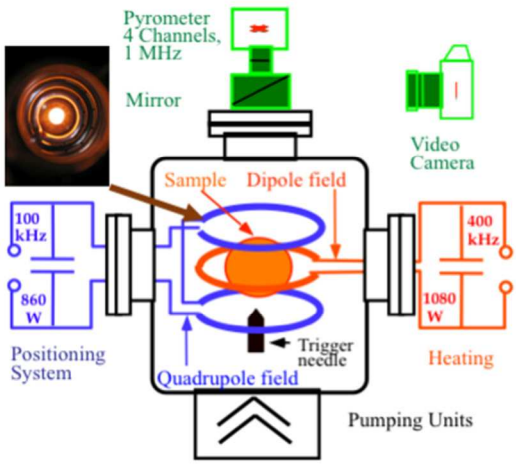

Figure 1: Schematic view of the TEMPUS facility. The heart of this facility consists of a quadrupole field for positioning and a diploe field for efficient heating. Experiments can be conducted under Ultra-High-Vacuum (HV) conditions in contrast to EML on Earth.

Levitation experiments allow for measurements of temperature-time-profiles during an entire undercooling and solidification experiment. The strong electromagnetic field needed to compensate the gravitational force causes

[1] Abbreviation of "Non-EQUIlibrium SOLidification, Modelling for Microstructure Engineering of Industrial Alloys"

strong stirring effects in the liquid. These are essentially reduced if electromagnetic levitation technique is applied in reduced gravity. In the environment of Space the forces to compensate disturbing accelerations are of some orders of magnitude smaller compared with experiments on ground. A special instrument called TEMPUS[2] has been designed to provide means of containerless processing in space [9]. Opposite to levitation on Earth positioning and heating are separated in TEMPUS by placing the sample into the superposition of a quadrupole and a dipole field [10]. The quadrupole field serves as positioning and the dipole field for heating, respectively. This two-coil concept leads to a drastic improvement of the overall efficiency and allows for independent control of positioning and heating. The concept is illustrated in Figure 1. It shows the two coil systems together with a pyrometer to measure contactless the temperature and a high speed camera to record the rapid propagation of dendrites. The dendrite growth velocity is measured as a function of undercooling.

3. Modelling

A segregation model was developed to follow the transformation path of the alloy solidified by a containerless process, such as levitation or atomization. Because such an initial condition is more generally valid for the formation of equiaxed grain structures, it is of major technological relevance for all casting technologies. The model is presented in details elsewhere [11, 12]. It is based on an extension of previously introduced concepts [13, 14]. A global heat balance (assuming uniform temperature) coupled with total mass and solute mass balances (assuming constant and equal density of all phases) are considered. The system is made of an initial spherical liquid droplet at the alloy composition. Figure 2b gives a schematic of the solidification sequence. It successively includes cooling of the lone liquid $l^{(0)}$ that composes zone (0), growth of a mushy zone (1) after nucleation of the primary dendritic solid phase $s_1^{(1)}$, growth of a eutectic zone (2) after nucleation of a structure $s_2^{(2)}$. The later eutectic structure develops first in place of the interdendritic liquid $l^{(1)}$ and then in place of the remaining liquid $l^{(0)}$. Finally, cooling of the fully solid system takes place.

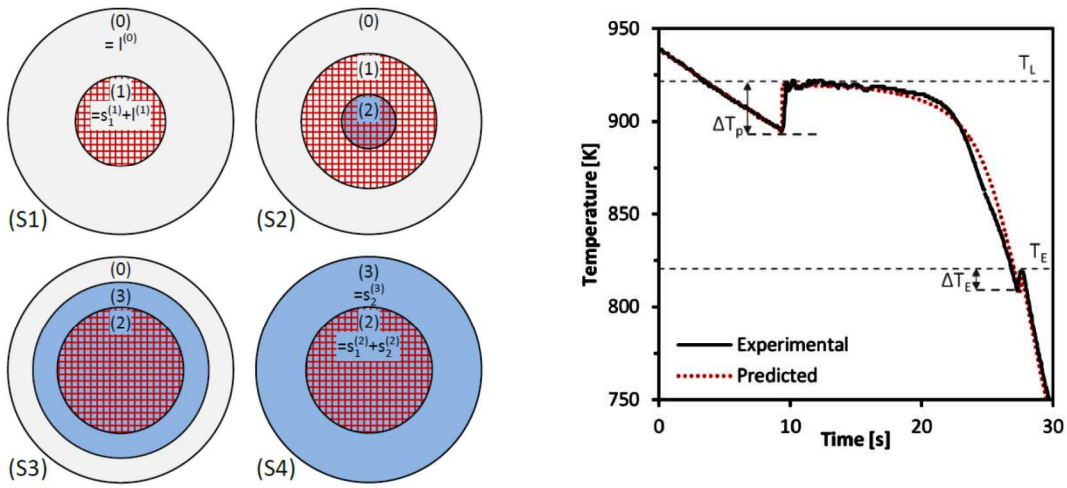

(a) (b)

Figure 2: (a) Schematized solidification sequence of a binary eutectic alloy (see text); (b) temperature-time profile measured by electromagnetic levitation and reproduced my modelling segregation.

The growth kinetics of the envelope of the mushy zone (1) and eutectic zone (2) are computed using sharp interface models of dendrite growth kinetics [15, 16] and the Jackson-Hunt eutectic theory [17], respectively. The interdendritic liquid $l^{(1)}$ located in the mushy zone is characterized by a high solute composition. It exchanges solute with the poorer extra-dendritic liquid $l^{(0)}$ located outside the mushy zone. Diffusion in the primary solid wphase s_1 is also accounted for. The model is fully coupled with thermodynamic equilibrium calculation [18].

[2] TEMPUS is a German acronym for Tiegelfreies Elektro-Magnetisches Prozessieren Unter Schwerelosigkeit

A sharp interface model [19, 20] has been recently extended to describe the growth dynamics of anisotropic dendrites with forced convection as a function of undercooling [21, 22]. The present model takes into account a change of the liquidus line and the slope of the liquidus line at high undercoolings because of kinetic reasons. In addition, influences of convection are integrated by introducing Peclet numbers for fluid flow and its impact on thermal and mass transport. These are mandatory to analyse the dendrite growth dynamics under the condition of forced convection as present in electromagnetic levitation experiments on Earth.

Phase-field modelling of microstructure evolution is based around an adaptive mesh multigrid solver for the coupled thermo-solutal system [23, 24]. The model is distinct from most other phase-field models as we do not require growth to be in an isothermal system, nor in an imposed temperature gradient, but rather the model solves the coupled equation set for the rejection of solute and latent heat into the liquid ahead of the growth front. As the ratio of thermal diffusivity, α, to solute diffusivity, D, (termed the Lewis number, Le), is typically >> 1, a range of advanced numerical methods are employed to cope with the resulting multiscale problem. These include:

1) Adaptive meshing refinement: This allows mesh cells to be located only in regions where the phase field, or one of the other fields, is varying significantly, typically close to the solid-liquid interface. The mesh refinement level is controlled by the gradients of the phase, solute and thermal fields.
2) Implicit time-stepping: Mesh adaptivity allows a highly refined mesh to be employed whilst retaining a moderate total element count. However, for the explicit forward Euler scheme employed in most phase-field codes this leads to restrictively small time-steps due to a stability criterion of the form $\Delta t \propto (\Delta x)^2$. This is overcome by using an implicit (2nd Order Backward Difference) time-stepping scheme which is unconditionally stable. However, at each time-step a large, but space, matrix system needs to be inverted.
3) Multigrid solver: Multigrid solvers are most efficient means of solving a large sparse system of equations, with the computational load scaling as $O(N)$, where N are the number of degrees of freedom. This compares with $O(N^2)$ for Gauss elimination or $O(N^{3/2})$ for successive over-relaxation or conjugate gradient methods.
4) Parallel execution: The system is built on the PARAMESH platform for execution on modern parallel HPC architectures.

The combined application of these numerical methods means that we operate the phase-field model at Lewis numbers approaching realistic values [25] and with a diffuse interface width.

4. Experimental results and discussion

Figure 3 shows the dendrite growth velocity as a function of undercooling of the $Al_{50}Ni_{50}$ intermetallic compound. Both results from terrestrial and experiments in reduced gravity are shown [26]. The green symbols represent measurements by using electromagnetic levitation on Earth with strong forced convection. The triangles, squares and pentagons give results of equivalent measurements in reduced gravity measured using the TEMPUS facility during several parabolic flight. The dashed line shows results of calculation within sharp interface theory neglecting convection whereas the solid line gives the corresponding results if fluid flow motion with velocities up to U_o=0.6 m/s are assumed comparable with magnetohydrodynamic computations [27] and experiments [28] for electromagnetically levitated drops on Earth.

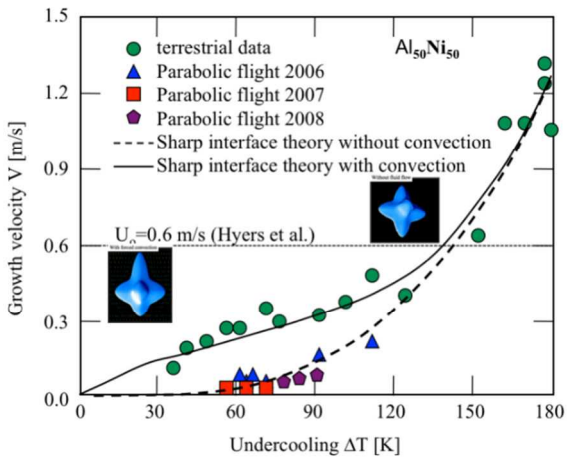

Figure 3: Dendrite growth velocity V as a function of undercooling measured of $Al_{50}Ni_{50}$, both under terrestrial (green circles) and µg conditions during parabolic flight missions using the TEMPUS facility (triangles, squares, pentagons). The dashed line gives the prediction of dendrite growth theory neglecting fluid flow while the solid line represents the prediction of dendrite growth theory assuming a fluid flow velocity of U_o=0.6m/s as determined by magneto-hydrodynamic simulation [**Error! Bookmark not defined.**].

The growth behaviour was experimentally investigated of $Al_{50}Ni_{50}$, $Al_{55}Ni_{45}$, $Al_{60}Ni_{40}$, $Al_{65}Ni_{35}$, $Al_{68.5}Ni_{31.5}$, $Al_{70}Ni_{30}$, $Al_{75}Ni_{25}$ alloy. The results are shown in Figure 4. In case of $Al_{50}Ni_{50}$ and $Al_{55}Ni_{45}$ the dendrite growth velocity increases monotonically with undercooling. An increase of Al-concentration by 5 at% leads to an essential change of the dendrite growth characteristics. A decrease of growth velocity is observed at undercoolings $\Delta T < 175$ K. The growth velocity passes a minimum and subsequently increases with rising undercooling. If the concentration of Al is further increased the minimum is shifted towards higher undercoolings [29].

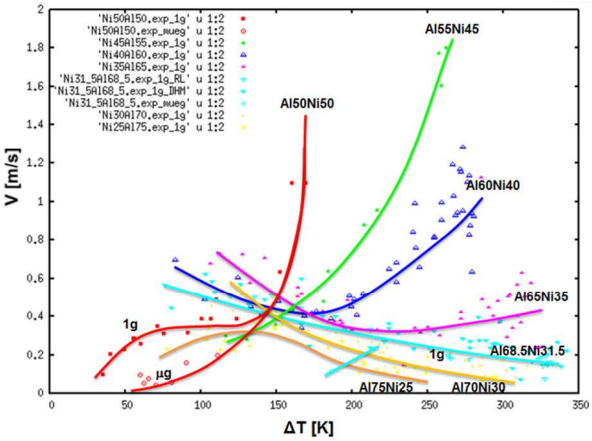

Figure 4: Dendrite growth velocity V as a function of undercooling ΔT of variously concentrated Al-Ni alloys. The lines show data trends as guide to the eye.

In order to investigate a possible influence of forced convection of the anomalous growth behaviour of Al-rich Al-Ni alloys the Raney type alloy $Al_{68.5}Ni_{31.5}$ was subject of various experiments in reduced gravity during TEXUS sounding rocket missions TEXUS 44 [30] and TEXUS 49 [31]. Figure 5 comprises the results of these investigations in direct comparison with results from 1g investigations.

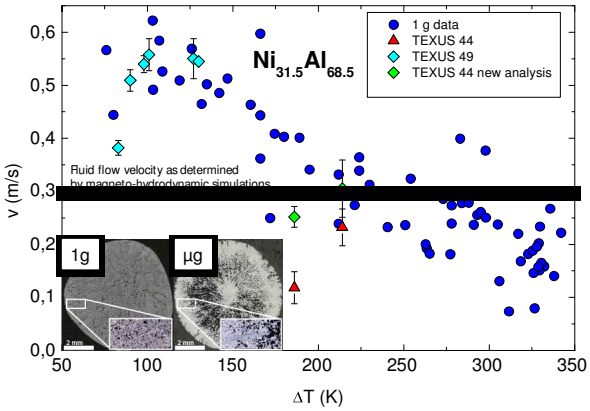

Figure 5: Dendrite growth velocity V versus undercooling ΔT of $Al_{68.5}Ni_{31.5}$ alloy, measured on Earth (blue dots) and in reduced gravity during TEXUS 44 mission (red triangles) and TEXUS 49 mission (light blue diamonds). The insert shows the microstructures of $Al_{68.5}Ni_{31.5}$ solidified at $\Delta T = 85$K on Earth (left) and in reduced gravity (right).

While the initial results of TEXUS 44 mission (red triangles) are different compared with the results obtained on Earth (1g) the results of TEXUS 49 mission (cyan diamonds) do not indicate a significant difference of both comparative sets of experiments. However, they are located in the regime where the growth velocity is larger than the estimated fluid flow speed $U_s \approx 0.3$ m/s induced by the electromagnetic fields in 1g (cf. dashed line) [27]. The experiments of the TEXUS 44 mission suffer from a low measuring frequency of the camera. The measuring frequency was enhanced by a factor of 4 during TEXUS 49 mission. A re-evaluation of the measurements on TEXUS 44 leads to values indicated by the green diamonds.

The insert of Figure 5 shows a significant difference of the microstructure of an $Al_{68.5}Ni_{31.5}$ sample solidified at an undercooling $\Delta T = 80$K under 1g (left) and in µg (right). The microstructure on the left exhibits grains without porosity whereas the microstructure on the right reveals great porosity in the volume and dendrites, which grow from a surface layer isotropically to the centre. From these observations it is concluded that solidification in reduced gravity may consist of two steps, first a layer on the surface is solidifying which acts as heterogeneous nucleation site for dendrites which grow to the centre of the sample.

NEQUISOL contributes two samples of $Al_{40}Ni_{60}$ to batch 1 of the EML experiments on board the ISS which were recently processed performing 25 solidification cycles successfully, 23 cycles for sample 1 and 2 cycles for sample 2. Both samples are of equal nominal compositions. Using sample 2 external triggering was successfully

applied to initiate solidification at small undercooling. Figure 6 shows the distribution of the nucleation undercooling measured. The average undercooling is inferred to be around ΔT=100 K. That is by about 70 K smaller than the maximum undercoolings measured for the same alloy by electromagnetic levitation under terrestrial (1g) conditions. So far it is not yet understood where this difference in maximum undercooling is coming from. There may be different effects which could be considered to explain this finding. The forced convection present in 1g experiments will hinder heterogeneous nucleation of a specific origin. In alloys the growth of an embryo to a nucleus of critical size is diffusion controlled. The atomic diffusion speed is in the order of 10 m/s. Hence it is rather unlikely that this effect explains the difference in nucleation undercooling in 1g and µg.

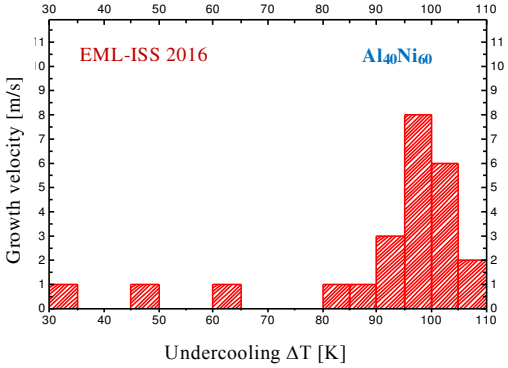

Figure 6: Distribution of nucleation undercooling as measured on $Al_{40}Ni_{60}$ alloy by electromagnetic levitation (EML) in reduced gravity on board the International Space Station (ISS).

The maximum undercoolings as measured both in 1g and µg are significantly smaller than estimated for the physical limit of the undercoolability as given by the onset of homogeneous nucleation. According to work by David Turnbull [32] the nucleation limit in the presence of homogeneous nucleation should be in the order of $\Delta T_{max} \approx 0.2\ T_L = 374$ K with $T_L = 1870$ K the liquidus temperature of $Al_{40}Ni_{60}$ alloy. Therefore, there must be a specific heterogeneous nucleation side being active in the levitation experiments.

In case of Al-based alloys it is well known that there is a strong tendency of Al in the liquid state of the alloy to form Al_2O_3 oxide. This oxide is very stable with a melting temperature of $T_L \approx 2350$ K and a boiling temperature of about 3225 K. If processing the Al-Ni alloy in an environmental gas atmosphere a solid Al_2O_3 layer is formed at the surface of the sample during heating within a time interval that is short compared with the processing time. In the present experiments the $Al_{40}Ni_{60}$ sample is processed in an Ar atmosphere of nominal purity of 6N at a pressure of 350 mbar. If one assumes a reaction probability of 1 (each individual reaction $4Al + 3O_2 = 2Al_2O_3$ is successful) a single surface layer of Al_2O_3 is formed at a pressure of 10^{-6} mbar within a time interval of 1 second. Under the present experimental conditions, the partial pressure of oxygen is in the order of 10^{-4} mbar. Therefore, the time for the formation of an Al_2O_3 surface layer is in the order of 10^{-2} seconds and, hence, is much smaller than the processing time in the order of several seconds. At temperatures T > 730 K a surface layer of Al_2O_3 is progressively formed which can act as an effective heterogeneous nucleation side. If the Al_2O_3 would be present during cooling the liquid sample will crystallize immediately if the temperature is falling below the liquidus temperature because of the high catalytic potency of Al_2O_3 for the formation of a heterogeneous nucleus of critical size.

T8here are chemical reactions which transfer the Al_2O_3 to AlO and Al_2O as investigated by Hoch and Johnston [33]. These are the following transformations:

$4\ Al + Al_2O_3 \rightarrow 3\ Al_2O$ at temperatures 1273 K < T < 1573 K

$1\ Al + Al_2O_3 \rightarrow 3\ AlO$ at temperatures T > 1873 K

Al_2O and AlO are highly volatile as shown by the same authors. An AlO sample in mass of 15 mg completely evaporates within 1 hour at a temperature of 2150 K. Therefore, a surface layer of Al_2O_3 in thickness of e.g. 10 nm may disappear within a time interval of a few seconds if the melt is heated up to 2170 K prior to cooling. Such a time interval is comparable with the experimental time for a heating and solidification cycle in the EML.

There is another transformation of Al_2O_3 that merits attention in the present discussion. Crystalline Al_2O_3, c-Al_2O_3, transforms to amorphous Al_2O_3, a-Al_2O_3 in the temperature regime 1000 K < T < 1300 K. Since both solid phases have different mass densities of 3.2 g/cm^3 in case of c-Al_2O_3 and 3.98 g/cm^3 in case of a-Al_2O_3 a solid Al_2O_3 layer may crack upon heating an Al-Ni sample forming nanosized Al_2O_3 clusters which can dissolve

into the liquid sample and can act as heterogeneous nucleation sides within the volume of the liquid alloy [34]. The curvature of the nm particles determines the catalytic potency of these heterogeneous nucleation modes [35]. The dissolution of the particles with respect to their distribution inside the liquid depends on the fluid flow motion and can affect the maximum undercooling and may be one reason for the different undercoolings measured in 1g and µg. Further on, also the liquid of the metallic melt in contact with the solid layer of Al_2O_3 develops an ordering within some interatomic distances as evidenced by investigations on undercooled pure Al [36]. This ordering affects the nucleation undercooling as discussed by Greer [37]. It can be speculated that this ordering mechanism depends on the fluid flow motion inside the melt and therefore affects the nucleation undercooling. All of these aspects shall be investigated in more detail to understand the different undercoolings of liquid $Al_{40}Ni_{60}$ alloy as measured in 1 g and µg, respectively.

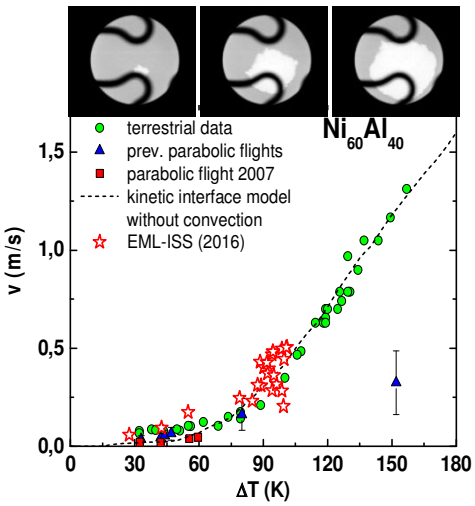

Figure 7: The dendrite growth velocity V as a function of undercoolig ΔT of $Al_{40}Ni_{60}$ alloy, measured under terrestrial conditions (green circles), during parabolic flight missions (blue triangles, red squares) and on board the International Space Station using the EML (red open stars). The ingots in the upper part display three pictures taken by the high speed camera at subsequent steps of solidification.

In addition to the nucleation issue also the dendrite growth velocity kinetics was investigated in the EML-ISS experiments of $Al_{40}Ni_{60}$ alloy. For doing so the concept as described in detail elsewhere has been applied to determine the velocity of the solidification front that propagates through the volume of the sphere-like sample [38]. In the previous experiments both on Earth and during parabolic flight missions the growth velocity was directly inferred from the propagation speed of the intersection line of the solidification front with the sample surface. This data is therefore afflicted with a systematic error which is under investigation by re-evaluating the previous experiments using the method. Figure 7 shows the preliminary evaluation of the dendrite growth velocity as a function of undercooling (red stars) as measured on $Al_{40}Ni_{60}$ alloy during the EML experiments on board the ISS. These measurements are compared with previous results of measurements of the dendrite growth velocity both during parabolic flight missions (blue triangles and red squares) and in the Earth laboratory (green circles). The upper part of the figure 7 displays three photographs taken by the high speed camera at subsequent steps during solidification. The solid part appears brighter than the liquid because the solidified part is heated up due to the release of the heat of fusion. According to Figure 7 no essential difference can be detected for all measurements within the scatter of the data. There is one exception. During a previous parabolic flight mission, the same alloy was processed using the TEMPUS facility. It succeeded to record one value of the dendrite growth velocity at an undercooling of 150 K. This value is significantly smaller than the value of the dendrite growth velocity measured at the same undercooling under terrestrial conditions.

5. Phase identification in Al-Ni alloys

AlNi alloys are important to the catalysis industry. The activity of Raney nickel catalyst is strongly affected by the morphology and weight fraction of Al_3Ni in the structure. $Al_{68}Ni_{32}$ and $Al_{79}Ni_{21}$ were atomized using IA in both helium and nitrogen gases. The microstructure of a range of powder sizes was examined quantitatively using Neutron Diffraction and SEM [39, 40, 41]. Similar compositions were slowly cooled (0.08 and 0.33 K/s) in a Differential Scanning Calorimeter (DSC) and microstructural examination. Also, an $Al_{68}Ni_{32}$ droplet was processed using the TEXUS sounding rocket which provided 320 seconds of reduced microgravity. The sample from the TEXUS flight was examined using Neutron Diffraction and SEM. Identification and quantification of the Al_3Ni_2 and Al_3Ni phases was carried out.

Comparing the phase quantification of Al_3Ni_2 and Al_3Ni for the IA, DSC and TEXUS samples revealed that cooling rate played a major role in the formation of these phases and their phase fractions.

Figure 8 shows the ratio of Al_3Ni/Al_3Ni_2 versus cooling rate for both $Al_{68}Ni_{32}$ and $Al_{79}Ni_{21}$ alloys processed using EML, IA and DSC [42]. The work of Patchett and Abbaschian is also shown in Figure 8. For the $Al_{68}Ni_{32}$ alloy, the ratio of Al_3Ni/Al_3Ni_2 appears to decrease with increasing cooling rate and then increase again. Also the ratio is higher than for $Al_{79}Ni_{21}$ alloy and the trend with increasing cooling rate is the opposite. As the cooling rate increases, the ratio of Al_3Ni/Al_3Ni_2 increases and appears to reach a maximum at around 100 K/s. Thereafter the ratio decreases with increasing cooling rate. The results seem to suggest that coarser sized powders may offer the optimum ratio of Al_3Ni/Al_3Ni_2 for catalyst performance.

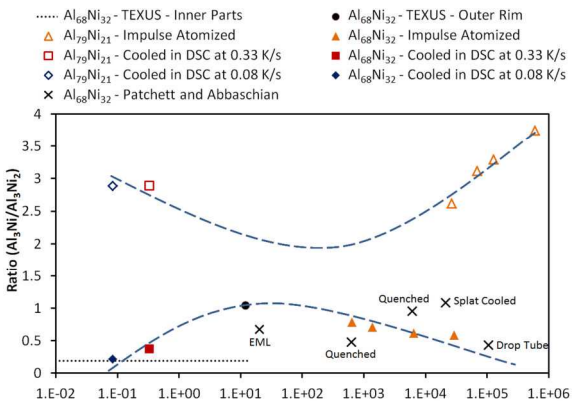

Figure 8: The Al_3Ni/Al_3Ni_2 ratio as a function of cooling rate for $Al_{68}Ni_{32}$ and $Al_{79}Ni_{21}$ samples produced using IA, DSC (0.08 and 0.33 K/s) and EML during TEXUS 44 campaign ($Al_{68}Ni_{32}$ only), as well as results reported by Patchett and Abbaschian for $Al_{68}Ni_{32}$ [43]. The measured cooling rate of the TEXUS sample (Outer Rim) varies from 14 K/s before solidification to 10 K/s after. The inner parts cooling rate (dotted line) is unknown but is less than at the outer rim. The two dashed lines highlight the trends in Al_3Ni/Al_3Ni_2 ratio for the two compositions studied.

6. Summary and conclusion

It was demonstrated that solidification kinetics and microstructure evolution is very much influenced by changes in mass and heat transport due to forced convection during experiments under terrestrial conditions. These disturbing effects can be eliminated by careful analogous experiments in reduced gravity environment as demonstrated for measurements of dendrite growth velocity of undercooled Al-Ni alloy. Highly accurate measurements in reduced gravity are therefore a mandatory requirement to quantitatively verify solidification models in particular in the regime of crystallization velocities being of comparable order of magnitude of the fluid flow velocity induced by forced convection. The upcoming period of the use of the International Space Station opens up a new area of research in which continuous and long duration series of experimental investigations in reduced gravity become possible.

Acknowledgment
We thank ESA for financial support of all institutions listed on the cover page. DMH thanks the German Research Foundation DFG for additional support within the contract HE1601/26. P.K.G. is grateful to the German Space Center Space Management under contract number 50WM1541 and the Russian Science Foundation under contract number 16-11-10095 for financial support.

References

[1] D. Turnbull, *Journal of Applied Physics* 1950, vol. **21**, pp. 1022-1029.

[2] J.H. Perepezko, *Materials Science & Engineering* 1984, vol. **65**, pp. 125-134.

[3] H.W.Kui, A.L. Greer, and D. Turnbull, *Applied Physics Letters* 1984, vol. **45**, pp. 615-618.

[4] F. Gillessen, D.M. Herlach, and B. Feuerbacher, B. (1988) *Zeitschrift für Physikalische Chemie* 1988, vol. **156**, pp. 129-136.

[5] D.M. Herlach, R.F. Cochrane, H.-J. Fecht, I. Egry, A.L. and Greer, *International Materials Review* 38**,** 273

(1993).

[6] D.M. Herlach, *Annual Review of Materials Science* 21, 23 (1991).

[7] D.M. Herlach and P.K. Galenko, *Mat. Sci. & Eng. A* 449-451, 34 (2007).

[8] D.M. Herlach, R. Lengsdorf, P. Galenko, H. Hartmann, Ch.-A. Gandin, S. Mosbah, A. Garcia-Escorial, H. Henein, Advanced Engineering Materials 10, 444 (2008).

[9] J. Piller, R. Knauf, P. Preu, G. Lohöfer, D.M. Herlach, *Proceedings 6th European Symposium on Materials Sciences under Microgravity,* ESA SP-256, 437 (1986).

[10] D.M. Herlach, G. Lohöfer, R. Willnecker, *German Patent, Patentschrift* DE 3639973 C2, (1989).

[11] Ch.-A. Gandin, S. Mosbah, Th. Volkmann, D.M. Herlach, *Acta Materialia,* 10, 444 (2008).

[12] D. Tourret, Ch. A. Gandin, Th. Volkmann, D. M. Herlach, *Acta Materialia*, 59, 4665 (2011).

[13] M. Rappaz, Ph. Thévoz, *Acta Metallurgica* 35, 2929 (1987).

[14] C.Y. Wang, C. Beckermann, *Metallurgical Transactions A* 24, 2787 (1993).

[15] R. Trivedi, J. Lipton and W. Kurz, *Acta Metall., 35* (1987) 965.

[16] W.J. Boettinger, S.R. Coriell and R. Trivedi, in R. Mehrabian and P.A. Parrish (eds.), *Rapid Solidification Processing: Principles and Technologies IV,* Claitor's, Baton Rouge, LA, 1988, p. 13.

[17] K.A. Jackson and J.D. Hunt, Transactions of the Metallurgical Society of AIME 236, 1129 (1966)

[18] PBIN: public binary alloys database, *Thermo-Calc Software AB*, Sweden (2008).

[19] P.K. Galenko and D.A. Danilov, *Phys. Lett. A*, 235, 271 (1997).

[20] P.K. Galenko and D.A. Danilov, *J. Cryst. Growth*, 197, 992 (1999).

[21] P.K. Galenko, D.A. Danilov, K. Reuther, D.V. Alexandrov, M. Rettenmayr, D.M. Herlach, *J. Cryst. Growth*, 457, 349 (2017).

[22] D.V. Alexandrov and P.K. Galenko, *Phys. Rev. E*, (2017) accepted for publication.

[23] P.C. Bollada, C.E. Goodyer, P.K. Jimack, A.M. Mullis & F.W. Yang, *J. Comp. Phys.* 287, 130 (2015).

[24] P.C. Bollada, C.E. Goodyer, P.K. Jimack & A.M. Mullis, *Appl. Phys. Lett.* 107, 053108 (2015).

[25] J. Rosam, P.K. Jimack and A. M. Mullis, *Phys. Rev. E* 79, 030601 (2009).

[26] S. Reutzel, H. Hartmann, P.K. Galenko, S. Schneider, D.M. Herlach, *Appied Physics Leters* 91, 041913 (2007).

[27] R.W. Hyers, *Meaurement Science and Technol*ogy 16, 394 (2005).

[28] J. Lee, D.M.Matson, S. Binder, M. Kolbe, D.M. Herlach, R.W. Hyers, *Metallurgical and Materials Transactions B* **45** (2014) 1018-1023. DOI: 10.1007/s11663-013-9995-5.

[29] R. Lengsdorf, D. Holland-Moritz, and D.M. Herlach, *Scripta Materialia* 62, 365 (2010).

[30] R. Lengsdorf, P.K. Galenko, and D.M. Herlach, (2009) *Report to DLR Space Management*,

[31] S. Klein and D.M. Herlach, (2012) *Report to DLR Space Management*

[32] D. Turnbull, *Contemporary Physics* 10, 473 (1969).

[33] M. Hoch and H.L. Johnston, *Journal of the American Chemical Society* 76, 2560 (1954).

[34] K. Kim, *Metallurgical and Materials Transactions A* 45, 3650 (2014).

[35] A.L. Greer, A.M. Brunn, A. Tronche, P.V. Evans, D.J. Bristow, , Acta Materialia 48, 2823 (2000).

[36] S.H. Oh, Y. Kauffmann, C. Scheu, W.D. Kaplan, M. Rühle. *Science* 310, 661 (2005).

[37] A.L. Greer, *Nature Materials* 5, 13 (2006).

[38] T. Volkmann, , in: *Solidification of Containerless Undercooled Melts*, editors D.M. Herlach and D.M. Matson, WILEY-VCH 2012, pp. 239.

[39] A. Ilbagi, P. Delshad Khatibi, I.P. Swanson, G. Reinhart and H. Henein, *Canadian Metallurgical Quarterly,* 50, 295 (2011).

[40] A. Ilbagi, H. Henein and A.B. Phillion, *J. Materials Science*, 46, 6235 (2011).

[41] A. Ilbagi and H. Henein, *Metallurgical and Materials Transactions A,* 45, 2152 (2014).

[42] A. Ilbagi, PhD Thesis, University of Alberta, (2012).

[43] J.A. Patchett and G.J. Abbaschian, *Proc. Fourth Conference on Rapid Solidification Processing: Principles and Technologies*, Edited by R. Mehrabian and P.A. Parish, U. of California, Santa Barbara, CA, USA (1986).